IEEE Access
Multidisciplinary | Rapid Review | Open Access Journal

Received March 7, 2019, accepted April 18, 2019, date of publication May 9, 2019, date of current version June 4, 2019.

Digital Object Identifier 10.1109/ACCESS.2019.2915982

Multidisciplinary Analysis and Multiobjective Design Optimization of a Switched Reluctance Motor for Improving Sound Quality

HYUNGWOO KIM[1], CAN NERSE[1], JONGSUH LEE[2], AND SEMYUNG WANG[1]
[1]School of Mechanical Engineering, Gwangju Institute of Science and Technology, Gwangju 61005, South Korea
[2]Department of Mechanical Engineering, Dong-A University, Busan 604-714, South Korea

Corresponding author: Semyung Wang (smwang@gist.ac.kr)

This work was supported by the National Research Foundation of Korea (NRF) through the Korean Government under Grant NRF-2017R1A2A1A05001326.

ABSTRACT In this study, the design optimization method for improving sound quality (SQ) of a switched reluctance motor (SRM) is proposed. The multidisciplinary finite element analysis (FEA) of an SRM is performed to evaluate both average torque and the SQ metrics to design the rotor configuration of the SRM. Specifically, the magneto-static FEA of the SRM is used to evaluate the average torque which is the most important performance of motors, and the local force distribution applied to the stator. Also, the transient structural FEA of the stator excited by the local force distribution, and the transient acoustic FEA are conducted to get the sound pressure radiated by the vibration of the stator. Then, the SQ metrics of loudness, sharpness, fluctuation strength and roughness can be obtained from the radiated sound pressure. We define the correlation function between the SQ metrics and the jury test results of the different types of SRMs. The weighted sum of the torque and the correlation function is set as an objective function. After that, design optimization method of the SRM using a design of experiments is discussed. This study does not consider the nonlinear material properties and is based on 2D analysis; however, with all these limitations, note that this is the first study to propose an overall procedure to increase the SQ of an SRM.

INDEX TERMS Design optimization, multidisciplinary finite element analysis, sound quality, switched reluctance motor.

I. INTRODUCTION

A Switched Reluctance Motor (SRM) has high efficiency and high torque density without rare earth material. In addition, the structure is simple [1], and operation is possible over a wide speed range [2]. Compared to brushless DC motors and interior permanent magnet synchronous motors, which use rare earth materials, SRMs can be competitive in terms of price and environment.

However, since the SRM has a doubly salient structure, it generates large vibration and noise [3]. In order to commercialize and popularize SRMs, vibration and noise problems of SRMs should be improved. Particularly, the demand related to the noise of the consumer of the product continues to increase, and the noise of the product greatly affects the purchase of the consumer. Therefore, the evaluation of SRM's noise experienced by humans and the study for its control are essential procedures in design stage of SRMs.

The degree to which humans feel about noise is difficult to be expressed. Sound Quality (SQ) metrics which can be calculated from the sound pressure were developed historically by psychoacoustic researchers as an objective indicator of human's subjective feelings of sound [4]–[8]. There are many metrics of SQ, which are loudness [5], sharpness [6], fluctuation strength [7], roughness [8], and so on. Many studies have been carried out to consider the SQ metrics [9]–[11]. However, no design studies related to the SQ of the SRM have been performed before.

There have been many researches related to the noise reduction of SRMs. The primary noise source of an SRM was investigated [3]. According to [3], the main cause of the noise emitted from the SRM is the radial attractive force generated between the stator and the rotor. This force is an exciting force that causes an oscillation of the stator and eventually

The associate editor coordinating the review of this manuscript and approving it for publication was Zhonglai Wang.

generates a sound field in the outward direction of the stator. The vibration and acoustic analysis with experiments of SRMs have been performed [12]–[14]. They solved eigenvalue problems and obtained the sound power level by using a mode superposition method. Using this method, the dynamic response of the stator structure can be approximated by a small number of its eigenmodes. Generally, however, the full transient method is more accurate than the mode superposition method and it is easy to use, since it does not require the number of eigenmodes and what eigenmodes without any references. Here, the transient analysis is necessary to apply SQ metrics which work in the time domain. Thus, in this work, we analyze vibration and noise of an SRM using the full transient method.

Also, design optimization studies have been carried out to reduce the noise of SRMs [15]–[18]. Most of design optimization studies have focused on indirect causes of noise, such as torque ripple, rather than directly handling the sound pressure radiated from the stator. However, the results of such optimization studies cannot easily predict exactly how much the radiated sound pressure has been reduced and the result design may differ from a design in which the radiated sound pressure is directly considered and reduced. Furthermore, the design which does not consider the sound pressure cannot consider SQ metrics. For this reason, to improve the SQ of SRMs, it is necessary to obtain the sound pressure radiated from the SRM in the time or frequency domain.

On the other hand, when designing to reduce the noise of the SRM, the average torque should be evaluated to prevent the decrease in average torque. As an extreme example, the average torque is zero when the motor is not running, and it certainly does not generate the noise. Thus, also the average torque should be evaluated and considered in the design optimization process.

Note that this work presents early and general design procedures of an SRM to improve the SQ based on multidisciplinary simulations. We evaluate the average torque, and the sound pressure radiated from the stator to obtain the SQ metrics which are loudness, sharpness, fluctuation strength and roughness from the radiated sound pressure of an SRM. In order to evaluate the average torque, we perform a magnetostatic Finite Element Analysis (FEA). Also, based on the input currents during actual operation, other magnetostatic FEAs are performed to obtain a local force distribution acting radially on the inner surface of the stator at each angle of the rotor position. A transient structural FEA of the stator is carried out by using these radial forces as excitation forces to obtain the acceleration in the radial direction of the outer surface of the stator. Next, regarding these radial accelerations as input sources, the transient acoustic FEA is conducted to evaluate the radiated sound pressure at the receiving point 1 m away from outside the stator. Then, by using LMS Test.Lab, SQ metrics are calculated from the sound pressure data. Finally, we conduct design optimization of an SRM to increase the average torque and to reduce the annoyance defined by correlation between SQ metrics and jury test results.

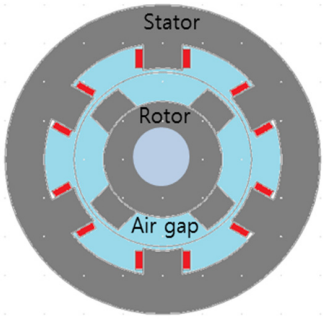

FIGURE 1. 6/4 Switched reluctance motor at unaligned rotor position.

II. MULTIDISCIPLINARY FINITE ELEMENT ANALYSIS

A. AVERAGE TORQUE

As mentioned in section I, the average torque has to be evaluated in order to prevent it from reducing in the design optimization process. To calculate the torque, the inductance should first be obtained. The inductance is a characteristic of a magnetic circuit, independent of the input current and is a function of rotor position. As shown in Fig. 1, in case of the 6/4 SRM, the entire magnetic circuit has exactly the same geometry at 90 degrees rotating intervals, and the inductance values are symmetrical with respect to 45 degrees. The discrete inductance values are calculated by magnetostatic FEA incrementally from 0 to 45 degrees, and linear interpolation is performed. Then, a line segment inductance function can be obtained. Additionally, by using a Fourier series approximation, we can obtain an explicit expression for the inductance curve at all rotating angles [18]. The magnetostatic FEA is performed using the governing equation of the 2D magnetostatic problem to obtain the magnetic vector potential in the z direction, A_z.

$$\frac{1}{\mu}\left(\frac{\partial^2 A_z}{\partial x^2}+\frac{\partial^2 A_z}{\partial y^2}\right)=-J \tag{1}$$

where x, y and, z are coordinates, J is the current density, μ is the permeability.

Then, the discrete inductance value at any rotor position can be calculated using (2).

$$l=\frac{1}{i^2}\int_{\text{allspace}}\frac{B^2}{\mu}\,dS \tag{2}$$

where l is the inductance, i is the arbitrary input current, B is the magnetic flux density, and S is the area.

The permeability of the steel of the rotor and stator used for the example in this study is 1.9209×10^{-3} (H/m), and the current density applied to each coil area is 4.28571×10^{8} (A/m^2).

The discrete inductance values become a line segment inductance function $L_{(line)}$ using linear interpolation as

shown in (3).

$$L_{(line)j}(\theta) = \left(\frac{l_{j+1} - l_j}{\theta_{j+1} - \theta_j}\right)\theta + \left(l_j - \frac{l_{j+1} - l_j}{\theta_{j+1} - \theta_j}\theta_j\right) \quad (3)$$

where the subscript j is the order of the rotating angle, and θ is the rotating angle.

Fig. 1 shows the unaligned position of the rotor, which is the initial position where $\theta = 0$. The inductance value is symmetrical with respect to 45 degrees, so the inductance curve $L(\theta)$ can be obtained for all angles from the following even function of the Fourier series approximation, given in (4), (5), and (6).

$$L(\theta) = L_0 + \sum_{n=1}^{NF} L_n \cos(nP_r\theta) \quad (4)$$

$$L_0 = \frac{1}{2\pi/P_r}\sum_{j=1}^{m}\left(\left(l_{j+1}+l_j\right)\left(\theta_{j+1}-\theta_j\right)\right) \quad (5)$$

$$L_n = \frac{2}{n\pi}\sum_{j=1}^{m} \times \left[\begin{array}{l} l_{j+1} \times \left(\sin(nP_r\theta_{j+1}) + \dfrac{\cos(nP_r\theta_{j+1}) - \cos(nP_r\theta_j)}{nP_r\left(\theta_{j+1} - \theta_j\right)}\right) \\ -l_j \times \left(\sin(nP_r\theta_j) + \dfrac{\cos(nP_r\theta_{j+1}) - \cos(nP_r\theta_j)}{nP_r\left(\theta_{j+1} - \theta_j\right)}\right) \end{array}\right] \quad (6)$$

where L_n is the coefficient of the $(n+1)$-th Fourier series term, P_r is the number of rotor poles, m is the number of piecewise line segments, and NF is the number of Fourier series terms.

To calculate the torque of the electric motor, the phase current should also be calculated, and the phase current can be obtained by solving the following voltage equation (7):

$$V = Ri + \frac{d\Phi(i,\theta)}{dt} \quad (7)$$

where V is the voltage, R is the resistance, and Φ is the magnetic flux linkage.

Assuming that the resistance is close to 0 and the voltage waveform is a single pulse, then the current phase i can be calculated using the following (8):

$$i(\theta) = \left\{\begin{array}{ll} \dfrac{V_0(\theta - \theta_{on})}{\omega\left(L_0 + \sum_{n=1}^{NF} L_n\cos(nP_r\theta)\right)} & (\theta_{on} \le \theta < \theta_{mid}) \\ \dfrac{V_0(\theta_{off} - \theta)}{\omega\left(L_0 + \sum_{n=1}^{NF} L_n\cos(nP_r\theta)\right)} & (\theta_{mid} \le \theta < \theta_{off}) \\ 0 & (\theta < \theta_{on}, \theta > \theta_{off}) \end{array}\right\} \quad (8)$$

where ω is the rotor angular velocity that is 1000 (rpm), V_0 is the reference voltage that is 300 (V), θ_{on} and θ_{off} are the on and off rotor angles, respectively, and θ_{mid} is $(\theta_{off} - \theta_{on})/2$.

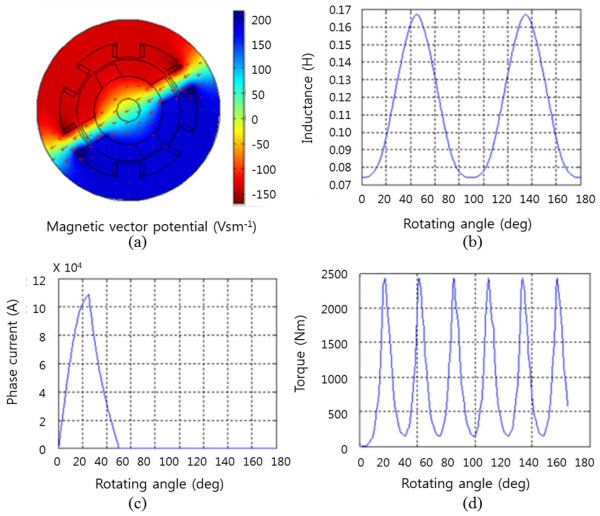

FIGURE 2. Torque calculation results: (a) magnetic vector potential (b) inductance (c) phase current (d) torque.

Generally, the torque T of the electric motor is calculated from the following (9):

$$T(i,\theta) = \frac{1}{2}i^2\frac{dL(\theta)}{d\theta} \quad (9)$$

By substituting the (4) and (8) with (9), a single-phase torque profile is obtained as shown in (10).

$$T(\theta) = \left\{\begin{array}{ll} \dfrac{1}{2}\left(\dfrac{V_0(\theta-\theta_{on})}{\omega\left(L_0+\sum_{n=1}^{NF} L_n\cos(nP_r\theta)\right)}\right)^2\left(-nP_r\sum_{n=1}^{NF} L_n\sin(nP_r\theta)\right) & (\theta_{on} \le \theta < \theta_{mid}) \\ \dfrac{1}{2}\left(\dfrac{V_0(\theta_{off}-\theta)}{\omega\left(L_0+\sum_{n=1}^{NF} L_n\cos(nP_r\theta)\right)}\right)^2\left(-nP_r\sum_{n=1}^{NF} L_n\sin(nP_r\theta)\right) & (\theta_{mid} \le \theta < \theta_{off}) \\ 0 & (\theta < \theta_{on}, \theta > \theta_{off}) \end{array}\right\} \quad (10)$$

In the case of the 6/4 SRM, the input current phase is changed at intervals of 30 degrees so that it is possible to evaluate the torque at all angles by superimposing the previously obtained torque by 30 degrees. The results of (1)-(10) to obtain the torque profile is shown in Fig. 2.

B. RADIATED SOUND PRESSURE

We can obtain the sound pressure radiated from the stator by performing the magnetostatic, transient structural, and transient acoustic FEAs. The analysis procedure for the radiated sound pressure is shown in Fig. 3.

For the vibration analysis of a stator, a force distribution applied locally to the inner surface of the stator is required rather than the net force that the whole stator receives. There are several methods to obtain the local force distribution, including the Maxwell stress tensor [19] and the equivalent

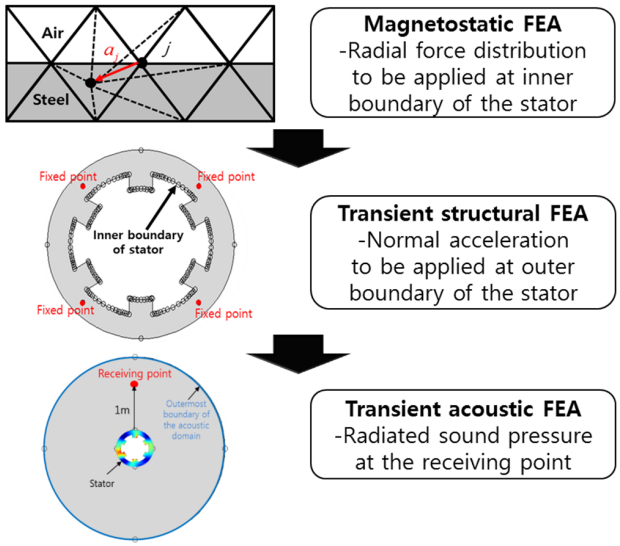

FIGURE 3. Multidisciplinary FEA procedure for radiated sound pressure.

source methods [20], [21]. Since the finite element solution follows the formula that minimizes the stored energy, the local virtual work method is suitable for the FEA [22]. Virtual work method is based on the principle of conservation of energy or co-energy and the principle of virtual displacement. We calculate the radial force distribution at all nodes of interface between the stator and air-gap using the local virtual work method. In Fig. 3, a_j shows the virtual movement of a node in the local virtual work method. The radial force distribution applied to the inner surface of the stator can be calculated using the following equations (11)-(13):

$$F_j = -\frac{\partial W}{\partial a_j}\bigg|_{\Phi=const} \tag{11}$$

$$F_j = -\frac{1}{2\mu}\mathbf{A}_z^{\mathrm{T}}\frac{\partial \mathbf{K}}{\partial a_j}\mathbf{A}_z \tag{12}$$

$$\begin{aligned}\frac{\partial \mathbf{K}}{\partial a_j} &= \iint \frac{\partial\,|\mathbf{J}|}{\partial a_j}\begin{bmatrix}\frac{\partial N_1}{\partial \hat{x}} & \frac{\partial N_1}{\partial \hat{y}}\\ \frac{\partial N_2}{\partial \hat{x}} & \frac{\partial N_2}{\partial \hat{y}}\\ \frac{\partial N_3}{\partial \hat{x}} & \frac{\partial N_3}{\partial \hat{y}}\end{bmatrix}\left(\mathbf{J}^{-1}\right)^{\mathrm{T}}\mathbf{J}^{-1}\\ &\quad\times\begin{bmatrix}\frac{\partial N_1}{\partial \hat{x}} & \frac{\partial N_2}{\partial \hat{x}} & \frac{\partial N_3}{\partial \hat{x}}\\ \frac{\partial N_1}{\partial \hat{y}} & \frac{\partial N_2}{\partial \hat{y}} & \frac{\partial N_3}{\partial \hat{y}}\end{bmatrix}dsdt\\ &\quad+\int\int|\mathbf{J}|\begin{bmatrix}\frac{\partial N_1}{\partial \hat{x}} & \frac{\partial N_1}{\partial \hat{y}}\\ \frac{\partial N_2}{\partial \hat{x}} & \frac{\partial N_2}{\partial \hat{y}}\\ \frac{\partial N_3}{\partial \hat{x}} & \frac{\partial N_3}{\partial \hat{y}}\end{bmatrix}\left(\mathbf{J}^{-1}\right)^{\mathrm{T}}\frac{\partial\left(\mathbf{J}^{-1}\right)}{\partial a_j}\\ &\quad\times\begin{bmatrix}\frac{\partial N_1}{\partial \hat{x}} & \frac{\partial N_2}{\partial \hat{x}} & \frac{\partial N_3}{\partial \hat{x}}\\ \frac{\partial N_1}{\partial \hat{y}} & \frac{\partial N_2}{\partial \hat{y}} & \frac{\partial N_3}{\partial \hat{y}}\end{bmatrix}dsdt\end{aligned}$$

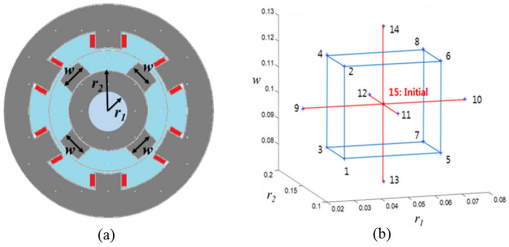

FIGURE 4. (a) 3 design variables of 6/4 SRM (b) CCD for 3 design variables.

$$+\iint|\mathbf{J}|\begin{bmatrix}\frac{\partial N_1}{\partial \hat{x}} & \frac{\partial N_1}{\partial \hat{y}}\\ \frac{\partial N_2}{\partial \hat{x}} & \frac{\partial N_2}{\partial \hat{y}}\\ \frac{\partial N_3}{\partial \hat{x}} & \frac{\partial N_3}{\partial \hat{y}}\end{bmatrix}\frac{\partial\left(\mathbf{J}^{-1}\right)^{\mathrm{T}}}{\partial a_j}\left(\mathbf{J}^{-1}\right)$$
$$\times\begin{bmatrix}\frac{\partial N_1}{\partial \hat{x}} & \frac{\partial N_2}{\partial \hat{x}} & \frac{\partial N_3}{\partial \hat{x}}\\ \frac{\partial N_1}{\partial \hat{y}} & \frac{\partial N_2}{\partial \hat{y}} & \frac{\partial N_3}{\partial \hat{y}}\end{bmatrix}dsdt \tag{13}$$

where F_j is the radial force at the j-th node, W is the virtual work, a_j is the virtual displacement at the j-th node, Φ is the flux linkage, the $\mathbf{K}$ is the stiffness matrix, $\mathbf{J}$ is the Jacobian matrix, $||$ is the determinant, the superscript T is the transpose operator, the superscript -1 is the inverse operator, N is the shape function, and $\hat{x}$ and $\hat{y}$ are local coordinates corresponding to x and y, respectively.

In the case of SRMs, although, magnetic saturation of iron could occur repeatedly in the operating condition, we assume that the permeability remains constant for ease of calculation. The local force is zero everywhere except at the interface of the airgap and stator. The fixed constant linkage Φ means fixed constant magnetic vector potential $\mathbf{A}_z$, therefore, only $\mathbf{K}$ is dependent on the virtual displacement a_j [23].

The radial force distributions at finite element nodes at the inner boundary of the stator are obtained by performing electromagnetic FEA from 0 to 30 degrees of the rotor position, and radial force distributions from 0 to 360 degrees in consideration of the periodicity of the operation by the phase change and the symmetricity of the geometry are obtained.

Next, the transient structural FEA is performed using the plane strain equations (14)-(17) to calculate the normal acceleration outside the stator.

$$\rho\frac{\partial^2 u}{\partial t^2} - \frac{\partial}{\partial x}\left((2G+\tau)\frac{\partial u}{\partial x}\right) - \frac{\partial}{\partial y}\left(G\frac{\partial u}{\partial y}\right) - \frac{\partial}{\partial x}\left(\tau\frac{\partial v}{\partial y}\right) - \frac{\partial}{\partial y}\left(G\frac{\partial v}{\partial x}\right) = F_x \tag{14}$$

$$\rho\frac{\partial^2 v}{\partial t^2} - \frac{\partial}{\partial y}\left((2G+\tau)\frac{\partial v}{\partial y}\right) - \frac{\partial}{\partial x}\left(G\frac{\partial v}{\partial x}\right) - \frac{\partial}{\partial y}\left(\tau\frac{\partial u}{\partial x}\right) - \frac{\partial}{\partial x}\left(G\frac{\partial u}{\partial y}\right) = F_y \tag{15}$$

$$G \equiv \frac{E}{2(1+\upsilon)} \tag{16}$$

$$\tau \equiv \frac{2\upsilon}{1-2\upsilon} \tag{17}$$

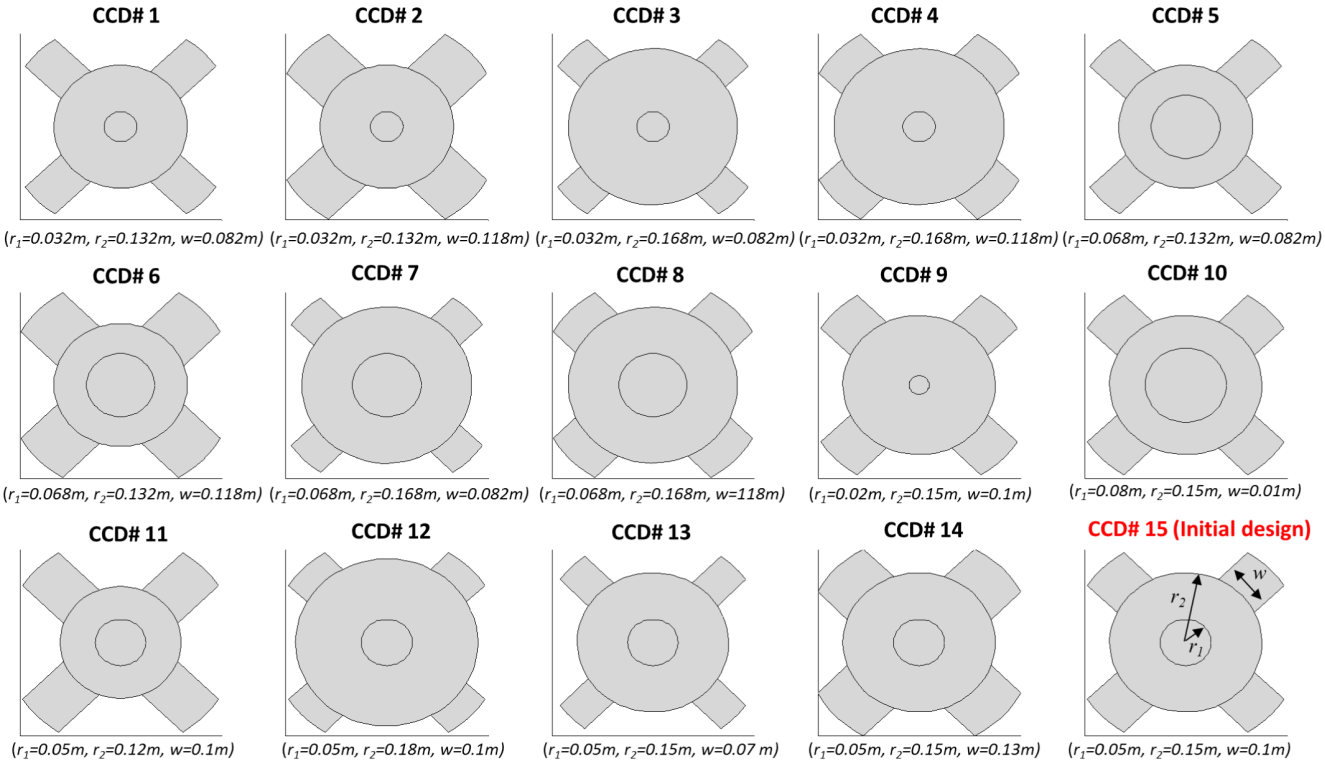

FIGURE 5. Rotor figurations for 15 CCD points.

where ρ is the mass density, t is the time, u and v are x and y direction displacement, respectively, E is the Young's modulus, and υ is the Poisson's ratio.

In order to consider the effect of the stator lamination in the 2D structural governing equations, we use the Young's modulus value 1.521×10^{11}(N / m) and the material density 7.293×10^{3}(kg / m^3) of steel [24].

Finally, a transient acoustic FEA is performed using the following acoustic wave equation (18):

$$\frac{1}{c_s^2}\frac{\partial^2 p}{\partial t^2} + \nabla \cdot (-(\nabla p)) = 0 \tag{18}$$

where c_s is the speed of sound, p is the acoustic pressure, and ∇ is the del operator.

To evaluate the acoustic pressure at the receiving point, which is 1 meter away from the stator, the acoustic domain is determined as shown in Fig. 3. The outer boundary of structural finite element domain is considered as the inner boundary of the acoustic finite element domain. It means the previously obtained normal acceleration values at the outer boundary of structural finite element domain are applied to the inner boundary of the acoustic finite element domain.

Since the acoustic analysis cannot be performed in the infinite region, the acoustic domain must be truncated to have a specific area. However, if we perform transient acoustic FEA without any boundary conditions, the outgoing acoustic wave will be reflected from the outermost boundary to the inside, and will be continuously accumulated. Therefore, boundary conditions such as a perfectly matched layer, a radiation boundary condition, or an impedance boundary condition should be applied to the outermost boundary to consider the free field [25]. We consider a free field in which an acoustic wave is naturally radiated by matching the impedance at the outermost boundary to have the same value by applying the impedance boundary condition (19):

$$\mathbf{n} \cdot \frac{1}{\rho_0}\nabla p + \frac{1}{Z}\frac{\partial p}{\partial t} = 0 \tag{19}$$

where $\mathbf{n}$ is the unit normal vector, ρ_0 is the air mass density, Z is the characteristic impedance.

C. SIMULATION RESULTS

Fig. 4 (a) shows 6/4 SRM with 3 design variables. The initial design variable is $r_1 = 0.05$, $r_2 = 0.15$, and $w = 0.01$. In section IV, we use the response surface method to solve the optimization problem. For this, we set three design variables to correspond to the central composite design (CCD) points as shown in Fig. 4 (b). Fig. 5 shows rotor figurations for 15 CCD points and Fig. 6 shows the radiated sound pressures of the SRM for 15 CCD points. Those 15 noise samples are used in section III.

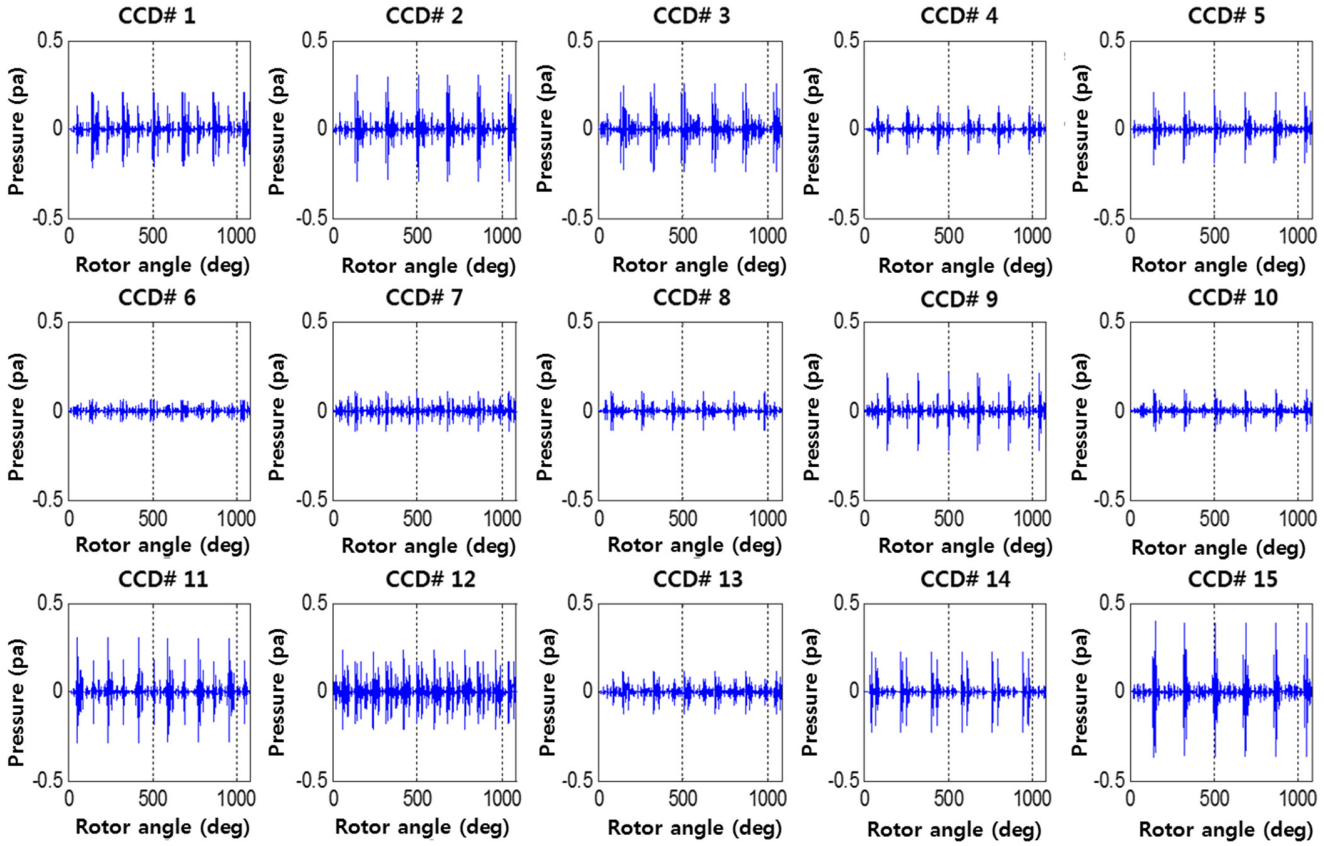

FIGURE 6. Sound pressures for 15 CCD points.

III. CORRELATION BETWEEN SOUND QUALITY METRICS AND JURY TEST

A. SOUND QUALITY METRICS

In this study, we want to express the noise annoyance experienced by people by considering four SQ metrics of the loudness, sharpness, fluctuation strength and roughness. The loudness represents the auditory perception relevant to the sound magnitude. Sharpness is the metric which represent sharpness of noise, and caused by high frequency noise components. Fluctuation strength and roughness indicate the degree of modulation of sound. These four SQ metrics are obtained by using LMS Test.Lab from the radiated sound pressures in the time domain. Table 1 shows the SQ metrics for 15 CCD points.

TABLE 1. Sound quality metrics.

CCD#	Loudness (sone)	Sharpness (acum)	Fluctuation Strength (vacil)	Roughness (asper)
1	8.99	1.60	0.29	2.07
2	9.50	1.60	0.31	2.19
3	10.38	1.64	0.33	1.72
4	5.77	1.65	0.29	0.82
5	8.45	1.58	0.29	2.03
6	6.73	1.60	0.21	0.95
7	6.89	1.63	0.23	0.46
8	5.63	1.61	0.26	0.71
9	8.19	1.60	0.38	1.81
10	7.88	1.51	0.28	2.38
11	11.40	1.61	0.43	2.48
12	9.83	1.60	0.27	1.27
13	8.01	1.58	0.24	0.85
14	11.11	1.66	0.39	2.54
15 (Initial)	10.29	1.58	0.37	2.61

B. JURY TEST

The jury test is carried out by 10 people. They are asked to listen to 15 different noise samples and evaluate the annoyance of the samples. The noise sample which is the least annoying is given score 1, and score 7 for the most annoying noise sample and obtained scores are shown in Table 2. Among the SQ metrics, loudness has the highest contribution to overall annoyance score according to people who took part in the jury test. For example, CCD# 8 which has the lowest loudness received the lowest annoyance score, whereas CCD# 14 which has the highest loudness received the highest annoyance score.

TABLE 2. Annoyance score.

CCD# \ Jury#	1	2	3	4	5	6	7	8	9	10	Sum
1	5	5	5	5	6	5	5	4	6	5	51
2	5	5	5	5	3	5	5	6	7	5	51
3	4	6	5	6	5	5	5	7	6	6	55
4	2	2	1	2	4	3	1	2	3	1	21
5	3	4	5	5	2	5	4	4	5	4	41
6	1	3	3	4	1	2	2	1	2	3	22
7	1	3	4	3	4	1	2	1	3	3	25
8	1	1	2	1	3	2	2	1	1	2	16
9	3	5	5	5	3	6	5	5	5	5	47
10	2	4	5	5	4	6	5	5	6	5	47
11	5	6	7	6	5	6	6	7	7	7	62
12	6	6	6	6	6	5	5	7	7	7	61
13	5	4	4	4	5	3	5	3	4	6	43
14	7	7	5	7	6	7	7	7	6	6	65
15 (Initial)	7	6	6	6	7	6	6	7	6	6	63

C. REGRESSION ANALYSIS FOR CORRELATION BETWEEN SOUND QUALITY METRICS AND JURY TEST RESULTS

The correlation between the SQ metrics and the jury test result is obtained by a linear regression model. The following equation forms 15 relations for 15 noise samples:

$$Ann_{score} = b_1 + b_2 \times Loudness + b_3 \times Sharpness + b_4 \times FluctuationStrength + b_5 \times Roughness \quad (20)$$

where Ann_{score} is the summation of annoyance scores in Table 2, b_j is the undetermined coefficient of j-th term.

The undetermined coefficients are determined by the least square method. Then, the noise annoyance index, Ann is defined as the following (21):

$$Ann = 103.68 + 9.4187 \times Loudness - 85.226 \times Sharpness + 20.359 \times Fluctuation\ strength - 0.5996 \times Roughness \quad (21)$$

For all CCD points, this equation is not supposed to predict the annoyance index exactly. The least percent error is 6% for CCD# 12 and the highest is 56% for CCD# 6, since it is too difficult to know exact formulation of the function of the Ann. The equation can be improved by tuning or deep learning techniques in future works.

IV. MULTI-OBJECTIVE OPTIMIZATION

A. OPTIMIZATION PROBLEM DEFINITION

The optimization problem is defined by (22)-(25).

$$Min \ \frac{Ann}{Ann_{initial}} - \frac{T_{avg}}{T_{avg}^{initial}} \quad (22)$$

$$S.t \ 0.02 \le r_1 \le 0.08 \quad (23)$$

$$0.12 \le r_2 \le 0.18 \quad (24)$$

$$0.07 \le w \le 0.13 \quad (25)$$

TABLE 3. Design of experiments.

CCD#	$\frac{Ann}{Ann_{initial}}$	$\frac{T_{avg}}{T_{avg}^{initial}}$	$\frac{Ann}{Ann_{initial}} - \frac{T_{avg}}{T_{avg}^{initial}}$
1	0.7735	1.1476	-0.3741
2	0.8487	0.8918	-0.0432
3	0.9247	1.0189	-0.0941
4	0.2766	0.8248	-0.5483
5	0.7278	1.1471	-0.4193
6	0.4492	0.8915	-0.4422
7	0.4409	1.0187	-0.5777
8	0.3039	0.8247	-0.5207
9	0.6965	1.0002	-0.3037
10	0.7400	0.9996	-0.2596
11	1.1313	1.0413	0.0899
12	0.8895	0.8587	0.0308
13	0.6626	1.1462	-0.4835
14	1.0087	0.7788	0.2299
15 (Initial)	1	1	0

TABLE 4. Initial and optimal results.

	Loudness (sone)	Sharpness (acum)	Fluctuation strength (vacil)	Roughness (asper)	$\frac{Ann}{Ann_{initial}}$	$\frac{T_{avg}}{T_{avg}^{initial}}$
Initial	10.29	1.58	0.37	2.61	1	1
Optimal	4.48	1.57	0.25	1.63	0.1899	1.1455

where $Ann_{initial}$ is the noise annoyance value of the initial design, T_{avg} is the average torque, and $T_{avg}^{initial}$ is the average torque of the initial design.

The noise annoyance index and average torque are divided into those of the initial model, respectively, for two reasons. The first is to normalize it to overcome the difference in scale between the annoyance and the average torque, and the second is to compare easily with the results of the initial model. Constraints are defined as side limits of each design variable.

B. RESPONSE SURFACE METHOD

We construct a design of experiments table as shown in Table 3. The response surface model is assumed as a second order polynomial, and the undetermined coefficients are determined by the least square method.

$$Y = h_1 + h_2 r_1 + h_3 r_2 + h_4 w + h_5 r_1 r_2 + h_6 r_2 w + h_7 w r_1 + h_8 r_1^2 + h_9 r_2^2 + h_{10} w^2 \quad (26)$$

where Y is the objective value, and h_j is the undetermined coefficient of j-th term.

As a result, the design variables for which the objective value is minimum are obtained as $r_1 = 0.0308$, $r_2 = 0.1692$, and $w = 0.0934$.

V. OPTIMIZATION RESULTS

Fig. 7 shows the rotor figurations, and Fig. 8 shows the torque profiles of the initial and optimized SRM. Compared with the

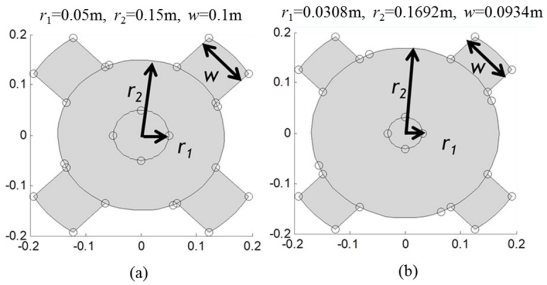

FIGURE 7. The rotor figurations: (a) initial model (b) optimized model.

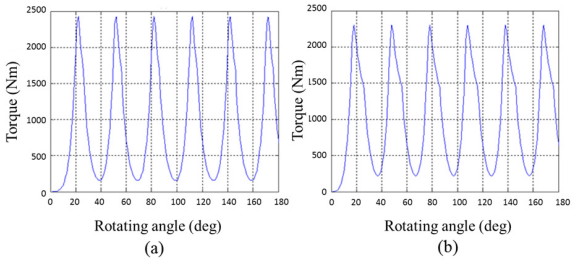

FIGURE 8. Torque profiles: (a) initial model (b) optimized model.

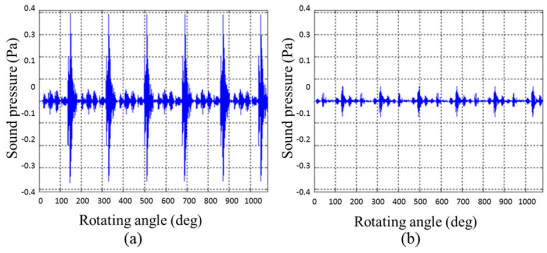

FIGURE 9. Radiated sound pressure: (a) initial model (b) optimized model.

initial model, the average torque was increased by 14.55% while the difference between maximum and minimum torque was reduced. This means that torque ripple was reduced. Fig. 9 shows the radiated sound pressures of the initial and optimized SRMs at the receiving point, and Table 4 shows the SQ metrics of the initial and optimized models. the noise annoyance index was reduced by 80.01%.

VI. CONCLUSION

In this study, the multidisciplinary design optimization of a 6/4 SRM was conducted to improve SQ. We obtained the SQ metrics and performed the jury test to consider the subjective opinion of the jury. We also defined the objective function to reduce the noise annoyance index and increase the average torque. The noise annoyance index was reduced by 80.01% and the average torque was increased by 14.55%. Therefore, the proposed design optimization procedure is successful to improve SQ of the SRM.

REFERENCES

[1] M. Krishnamurthy, C. S. Edrington, A. Emadi, P. Asadi, M. Ehsani, and B. Fahimi, "Making the case for applications of switched reluctance motor technology in automotive products," *IEEE Trans. Power Electron.*, vol. 21, no. 3, pp. 659–675, May 2006.

[2] R. B. Inderka, M. Menne, and R. W. A. A. De Doncker, "Control of switched reluctance drives for electric vehicle applications," *IEEE Trans. Ind. Electron.*, vol. 49, no. 1, pp. 48–53, Feb. 2002.

[3] D. E. Cameron, J. H. Lang, and S. D. Umans, "The origin and reduction of acoustic noise in doubly salient variable-reluctance motors," *IEEE Trans. Ind. Appl.*, vol. 28, no. 6, pp. 1250–1255, Nov. 1992.

[4] E. Zwicker and H. Fastl, *Psychoacoustics: Facts and Models*. Berlin, Germany: Springer-Verlag, 1990.

[5] H. Fletcher and W. A. Munson, "Loudness, its definition, measurement and calculation," *J. Acoust. Soc. Amer.*, vol. 5, no. 2, pp. 82–108, Oct. 1933.

[6] G. V. Bismarck, "Sharpness as an attribute of the timbre of steady sounds," *Acta Acustica United Acustica*, vol. 30, no. 3, pp. 159–172, Mar. 1974.

[7] P. Daniel and R. Weber, "Psychoacoustical Roughness: Implementation of an optimized model," *Acta Acustica United Acustica*, vol. 83, no. 1, pp. 113–123, Jan./Feb. 1997.

[8] H. Fastl, "Fluctuation strength and temporal masking patterns of amplitude-modulated broadband noise," *Hearing Res.*, vol. 8, no. 1, pp. 59–69, Sep. 1982.

[9] S.-I. Sato, J. You, and J. Jeon, "Sound quality characteristics of refrigerator noise in real living environments with relation to psychoacoustical and autocorrelation function parameters," *J. Acoust. Soc. Amer.*, vol. 122, no. 1, pp. 314–325, Jul. 2007.

[10] W.-H. Cho, J.-G. Ih, S.-H. Shin, and J.-W. Kim, "Quality evaluation of car window motors using sound quality metrics," *Int. J. Automot. Technol.*, vol. 12, no. 3, pp. 443–450, Jun. 2011.

[11] F. Lin, S. Zuo, W. Deng, and S. Wu, "Noise prediction and sound quality analysis of variable-speed permanent magnet synchronous motor," *IEEE Trans. Energy Convers.*, vol. 32, no. 2, pp. 698–706, Jun. 2017.

[12] J. O. Fiedler, K. A. Kasper, and R. W. De Doncker, "Calculation of the acoustic noise spectrum of SRM using modal superposition," *IEEE Trans. Ind. Electron.*, vol. 57, no. 9, pp. 2939–2945, Sep. 2010.

[13] F. L. M. dos Santos, J. Anthonis, F. Naclerio, J. J. C. Gyselinck, H. Van der Auweraer, and L. C. S. Goes, "Multiphysics NVH modeling: Simulation of a switched reluctance motor for an electric vehicle," *IEEE Trans. Ind. Electron.*, vol. 61, no. 1, pp. 469–476, Jan. 2014.

[14] X. Liang, G. Li, J. Ojeda, M. Gabsi, and Z. Ren, "Comparative study of classical and mutually coupled switched reluctance motors using multiphysics finite-element modeling," *IEEE Trans. Ind. Electron.*, vol. 61, no. 9, pp. 5066–5074, Sep. 2014.

[15] B. Mirzaeian, M. Moallem, V. Tahani, and C. Lucas, "Multiobjective optimization method based on a genetic algorithm for switched reluctance motor design," *IEEE Trans. Magn.*, vol. 38, no. 3, pp. 1524–1527, May 2002.

[16] Y. K. Choi, H. S. Yoon, and C. S. Koh, "Pole-shape optimization of a switched-reluctance motor for torque ripple reduction," *IEEE Trans. Magn.*, vol. 43, no. 4, pp. 1797–1800, Apr. 2007.

[17] S. I. Nabeta, I. E. Chabu, L. Lebensztajn, D. A. P. Correa, W. M. D. Silva, and K. Hameyer, "Mitigation of the torque ripple of a switched reluctance motor through a multiobjective optimization," *IEEE Trans. Magn.*, vol. 44, no. 6, pp. 1018–1021, Jun. 2008.

[18] J. Lee, J. H. Seo, and N. Kikuchi, "Topology optimization of switched reluctance motors for the desired torque profile," *Struct. Multidisciplinary Optim.*, vol. 42, no. 5, pp. 783–796, 2010.

[19] A. N. Wignall, A. J. Gilbert, and S. J. Yang, "Calculation of forces on magnetised ferrous cores using the Maxwell stress method," *IEEE Trans. Magn.*, vol. MAG-24, no. 1, pp. 459–462, Jan. 1988.

[20] H. S. Choi, I. H. Park, and S. H. Lee, "Generalized equivalent magnetizing current method for total force calculation of magnetized bodies in contact," *IEEE Trans. Magn.*, vol. 42, no. 4, pp. 531–534, Apr. 2006.

[21] H. S. Choi, S. H. Lee, and I. H. Park, "General formulation of equivalent magnetic charge method for force density distribution on interface of different materials," *IEEE Trans. Magn.*, vol. 41, no. 5, pp. 1420–1423, May 2005.

[22] H. S. Choi, I. H. Park, and S. H. Lee, "Concept of virtual air gap and its applications for force calculation," *IEEE Trans. Magn.*, vol. 42, no. 4, pp. 663–666, Apr. 2006.

[23] J. Lee, "Structural design optimization of electric motors," Ph.D. dissertation, Mech. Eng., Univ. Michigan, Ann Arbor, MI, USA, 2010.

[24] Z. Tang, P. Pillay, A. M. Omekanda, C. Li, and C. Cetinkaya, "Young's modulus for laminated machine structures with particular reference to switched reluctance motor vibrations," *IEEE Trans. Ind. Appl.*, vol. 40, no. 3, pp. 748–754, May 2004.

[25] C. K. W. Tam and L. Auriault, "Time-domain impedance boundary conditions for computational aeroacoustics," *Amer. Inst. Aeronaut. Astronaut.*, vol. 34, no. 5, pp. 917–923, May 1996.